Master of Science thesis

Dosimetrical studies on a tissue level using the MCNP4c2 Monte Carlo Simulations

Erik Larsson

Supervisors:

Bo-Anders Jönsson

Lena Jönsson

Michael Ljungberg

Per Munch af Rosenschöld

Department of Medical Radiation Physics

Lund University

Sweden

LUJI-RADFYS-EX-XXXX

TABLE OF CONTENTS

Abstract in Swedish

För att försöka uppskatta möjliga risker av joniserande strålning används begreppet absorberad dos, som är den absorberade energin per massenhet i ett organ. För radioaktiva läkemedel är absorberad dos inte direkt översättbart till risk, pga heterogena fördelningar av aktivitet på både vävnads- och cellnivå. Denna heterogenitet kan inte upptäckas med dagens gammakamera, då denna har en upplösning på ungefär 1 cm, eller ca 1000 cellradier. Den aktivitet man mäter är därmed ett medelvärde över ca 10^9 celler, och då kan man inte avgöra om aktiviteten är homogent eller heterogent fördelad i vävnaden.

För en del radioaktiva läkemedel kan en stor del av aktiviteten elimineras via tarmsystemet. Detta kan leda till att tarmväggen utsätts för höga doser. Problemet med tunntarmen är att tarmväggen är ca 3-6 mm tjock, och därför inte kan särskiljas från tarminnehållet mha gammakameran. Nuvarande använda modeller för beräkning av absorberad dos till tarmväggen bygger på att all aktivitet befinner sig i tarminnehållet. Detta gäller inte för alla radioaktiva läkemedel och andelen aktivitet i tarmvägg jämfört med aktivitet i tarminnehåll kan erhållas från djurförsök där aktiviteten i utdissekerad tarm resp. tarminnehåll mäts.

I denna studie har en ny tidigare publicerad tarmmodell (1) använts för att bestämma absorberad dos till de strålningskänsliga kryptcellerna i tarmväggen. Modellen tar hänsyn till aktivitetsupptaget i tunntarmsväggen och aktiviteten i tarminnehållet. Dessutom beräknas även dosbidraget från intilliggande tarmslingor. Då detta inte går att beräkna analytiskt har arbetet gjorts med s.k Monte-Carlo simuleringar som genom slumptal och sannolikheter för hur partikeln växelverkar med vävnaden simulerar en partikels väg, samt dess energideponering, i vävnaden. Genom att simulera tillräckligt många partiklar ger detta en bild av verkligheten.

Syftet med examensarbetet var att lära mig Monte Carlo-programmet MCNP4c2, dess teori, och begränsningar inom användningsområdet small-scale dosimetry. Detta har gjorts med hjälp av att reproducera och verifiera data från arbetet beskrivet ovan, i vilket ett annat Monte Carlo-programm använts, EGS4.

I detta arbetet simulerades först fotoner och elektroner med olika startenergier för att kunna dra samband vid simuleringen av sex intressanta radionuklider som sönderfaller med ett helt spektra av energier. Resultatet av arbetet var att de bägge Monte Carlo programmen ger ungefär samma resultat, dvs att nuvarande modeller för de studerade radionukliderna ganska kraftigt överskattar dosen till de känsliga kryptcellerna. Det viktigaste resultatet i dettta arbete är dock att jag nu kan tillämpa Monte Carlo programmet använt i denna studie på nya modeller av andra organ.

Abstract

The purpose of this thesis has been to learn the MCNP-code, its theory and limitations, and how to use it in the field of small-scale dosimetry. In order to evaluate the applicability of the code for future dosimetry studies it was applied on a novel small-intestinal dosimetry model (1).

For some radiopharmaceuticals a significant amount of activity is excreted through the gastrointestinal tract. It has also been shown that the activity may concentrate in the intestinal wall. The absorbed dose to the wall might therefore be significant and need to be considered in risk estimations relating to the radiopharmaceuticals. Since, the small intestinal wall is impossible to distinguish from the intestinal contents with modern nuclear medicine imaging; the general dosimetric models assume that all activity is located in the contents. This work is based on a model previously published to simulate S values to the radiosensitive crypt cells and *villi* in the small intestinal wall using Monte Carlo technique. The activity is assumed to be located in both intestinal contents and wall. The MC-program used in this work was the MCNP4c2- and MCNPX-code. The model calculates the contribution of nearby intestinal loops by assuming that the small intestine is a cylinder and that the intestinal loops build a hexagonal pattern. The work includes simulations with monoenergetic photons and electrons and the radionuclides ^{99m}Tc, ^{111}In, ^{131}I, ^{67}Ga, ^{90}Y and ^{211}At. The results verify that for radionuclides used in nuclear medicine the cross-dose from nearby loops are essential. It is also confirmed that the fraction of cumulated activity in the intestinal wall to the contents is of great importance in order to estimate the absorbed dose. It was stated that the MIRD-, MIRDOSE3- and ICRP-model tends to overestimate the absorbed dose to the intestinal wall.

Introduction

The aim of this thesis was i) to learn how to use the MCNP4c2-code in the field of small-scale dosimetry, ii) get into the theory behind it and limitations and iii) to apply the MCNP4c2-code on a geometry, previously simulated (1) using the EGS4-code, in order to compare the results from the two Monte Carlo simulations and resulting S values.

Internal dosimetry

Diagnostic imaging and radionuclide therapy in nuclear medicine are based on the concentration of the radionuclide in the organ of interest. The activity may also be present in other organs or tissues, and for therapy the absorbed dose to these organs may limit the activity need to administer to receive the expected effect. An accurate calculation of the absorbed dose and related effective dose is therefore essential for an estimation of possible risks using radiopharmaceuticals, whether they are used for diagnostic imaging, therapy or in metabolic studies.

Much attention has been given to specify absorbed dose for external beams used in diagnostic and therapeutic radiology, than has been devoted to internal exposures from nuclear medicine imaging and radionuclide therapy (2). Nuclear medicine was not widely used prior to the 1950s, and in especially for radionuclide therapy, more attention was given on the amount of radioactivity administered rather than the absorbed dose to critical organs and tissues. Theoretically, the absorbed dose could be as accurately calculated in nuclear medicine as in external beam dosimetry. This required that variation in time of the activity distribution of the radionuclide can be precisely measured. External beam therapy is based on a well-known relationship between the absorbed dose and the tissue response, even though the response may vary between patients. This correlation between absorbed dose and the effect is not as straightforward in internal dosimetry, mainly due to a possible heterogenic activity distribution in the tissue as well as on the cellular level. This non-uniformity of activity can not be determined by modern scintillation cameras, which have a spatial resolution of about 1 cm or 1000 cell radius. This is then equivalent to averaging the absorbed dose averaged over approximately 10^9 cells.

The activity distribution on a tissue- and cellular level can be determined by tissue samples from *e.g*. tissue biopsies from patients and from animals. The non-uniformity can be studied from *in vitro* samples by using autoradiographic techniques or biochemical methods (19). A better knowledge of the detailed activity distribution will subsequently increase the accuracy in the methods in order estimate the absorbed dose to different targets. A high accuracy may then lead to more well-defined absorbed-dose to tissue-response relation.

In addition, the absorbed dose to the organ using tabulated schemas values is an average over a volume containing about 10^9 cells/cm^3. Thus, the effect of a non-uniform activity distribution both on tissue and cellular-level is not accounted for. The distribution of the radiopharmaceutical could be studied with an invasive method called autoradiography. Thin slices of an organ are studied *in vitro* by placed them on a photographic film for exposure to obtain a high-resolution image of the activity distribution within the organ or for intracellular distribution with a light microscopy or electron microscopy. To correlate absorbed dose with effect on a tissue with non-uniform activity distribution, techniques which consider heterogenic activity distribution on both macro- and microscopic level must be developed.

The technology of today makes is possible to quantify the distribution of activity within an organ with better accuracy. With CT or MRI organ sizes and volumes can be determined. By

fusing a CT/MR-study with a SPECT- or PET-study the activity in a certain organ can be better determined. The problems with attenuation and scattered radiation in patient, collimator and detector can not completely be eliminated and this degrades the images. With the fast computers of today many methods to correct the images for activity quantification has been developed or is under development.

MIRD-formalism

The general formalism for calculating the absorbed dose in internal dosimetry is the MIRD schema (3). This schema reduces the rather complicated calculations to a few parameters, *i.e.*

$$\overline{D} = \tilde{A} \cdot S \qquad \text{(Egn. 1)}$$

The parameters that determines the absorbed dose to a specific organ *k* are

- the administered activity, A_0,
- the physical half-life of the radionuclide, T_{fys},
- the distribution in time of the radioactivity in the specific organ r_k (target) and, if the radiation is penetrating, in other organs r_h (sources),
- the emitted mean energy per decay Δ,
- the fraction of the emitted energy deposited in the organ r_k from different sources r_h, $\varphi(r_k \leftarrow r_h)$.
- The mass of the target organ m_k

The first three parameters for an organ *h* form the quantity called cumulated activity $\tilde{A}_h$, which is the total number of decays in an organ *h* during the time interval of interest (Eqn. 2)

$$\tilde{A}_h = \int_{t_1}^{t_2} A_h(t)dt \qquad \text{(Eqn. 2)}$$

The last three parameters defined above describe the physical properties of the emitted radiation. These are substituted into a so called S value, *i.e.* mean absorbed dose per unit cumulated activity from a source volume r_h to a target volume r_k (Eqn. 3).

$$S(r_k \leftarrow r_h) = \frac{\varphi(r_k \leftarrow r_h)}{m_k} \cdot \Delta \qquad \text{(Eqn. 3)}$$

These two equations multiplied are sufficient to describe the mean absorbed dose delivered to the target volume *k* from a source volume *h* and the relation is given by Eqn. 4.

$$D(r_k \leftarrow r_h) = \tilde{A}_h \cdot S(r_k \leftarrow r_h) = \int_{t_1}^{t_2} A_h(t)dt \, \frac{\varphi(r_k \leftarrow r_h)}{m_k} \cdot \Delta \qquad \text{(Eqn. 4)}$$

The total absorbed dose to the target r_k from all sources r_h can be written as (Eqn. 5).

$$D(r_k) = \sum_h D(r_k \leftarrow r_h) \qquad \text{(Eqn. 5)}$$

The cumulated activity Ã

The activity in a source volume depends on the uptake and retention of the radio-pharmaceutical, as well as the physical half-life of the radionuclide. The biological parameters differ from patient to patient. To estimate the absorbed dose delivered in a diagnostic study to a population of patients, standard residence times found in literature (ref) are used. To quantify the cumulated activity in the introduction of a new radiopharmaceutical for diagnostic or therapeutic purposes the biological parameters must be studied in detail. Therapy involves radionuclides emitting non-penetrating radiation and higher activities resulting in higher absorbed doses. Thus, the biokinetics must be determined before the treatment in order to

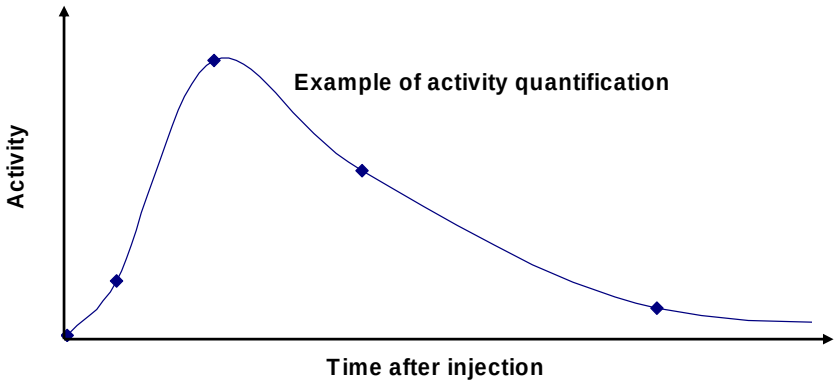

Figure 1. Schematic time-activity curve. The Ã is the area under the curve.

know the amount of activity to administer. For this purpose the radiopharmaceutical is labeled with a radionuclide that emits penetrating radiation, *i.e.* gamma radiation. It is then assumed that the radionuclide does not affect the carrier molecule and the biological distribution remains the same if the pharmaceutical is labeled with another radionuclide. Whole-body activity quantifications with scintillation cameras are used to obtain such information. Ideally, many measurements would be performed for an accurate determination of the cumulative activity. For practical and economical reasons, activity quantifications are usually limited to a few measurements (2). The time-activity curves are obtained by drawing region-of-interests over the source volume/area in the scintillation camera images. Single- or multiple-exponential curves are often used to fit the data as accurate as possible. The cumulated activity is finally calculated as the area under the curve, *i.e.* integrating over the entire time period range [0, ∞]. A schematic example of a time-activity curve is shown in Fig. 1.

A different representation of the cumulated activity in a target volume *h* is the *residence time,* τ_h (3) defined as $\tau_h = \tilde{A}_h / A_0$ where A_0 is the administered activity. Multiplication with the *S* value then gives the mean absorbed dose per administrated activity.

S values

The complete equation of calculating an S value is expressed as

$$S(r_k \leftarrow r_h) = \sum_i \Delta_i \Phi_i (r_k \leftarrow r_h) \qquad \text{(Eqn. 6)}$$

where

- $\Delta_i = n_i E_i$ is the mean energy of type *i* emitted per nuclear transition
- $\Phi_i(r_k \leftarrow r_h) = \frac{\varphi_i(r_k \leftarrow r_h)}{m_k}$ is the specific absorbed fraction, and is defined as the fraction of energy absorbed in target volume *k* emitted from source volume *h* for the *i*-type radiation.

The mean energy is given in the literature (4, 5). The specific absorbed fraction generally depends on the geometry of the patients but tabulated fractions are calculated by Monte Carlo simulations using various mathematical phantoms. Standard S values or specific absorbed fraction for numerous radionuclides have been simulated for many organs, and are tabulated by ICRP (6) and MIRD (7). These data have then been compiled into a computer program MIRDOSE3 (8) that is generally available and has then been developed to simplify the calculation of absorbed dose per unit administered activity.

The tabulated S values are calculated using different computer phantoms. Organ sizes and patient lengths and weights etc or different individuals can differ significantly comparing to the computer phantoms, and the true S value for each patient will not be equal as the pre-calculated and tabulated values. One method to partly compensate for this difference is to apply scaling techniques in order to make the S values more appropriate to a particular patient.

Alpha-particles

Since α-particles are densely ionizing, the relative biologic effect is large as compared to electrons and photons. Because of the short range of the α-particles, tumor targeting α-emitters could be useful for therapy purposes since normal tissue surrounding the target of interest could be spared.

The small intestine and its dosimetric models

Most of the digestion and absorption of water and nutrients occurs in the small intestine. The mucous membrane forms cylinder shaped folds, called *villi*, and on these folds small micro-*villi* are attached. This Muscularisshape creates a big enlargement of the intestinal wall-surface in favor of the absorption. Due to the non-friendly environment in the small intestine, the lifespan of the *villi* is short and they are constantly being renewed. This is made by the crypt cells, located at the bottom of the *villi*. These cells are undifferentiated stem cells, and radiosensitive (9).

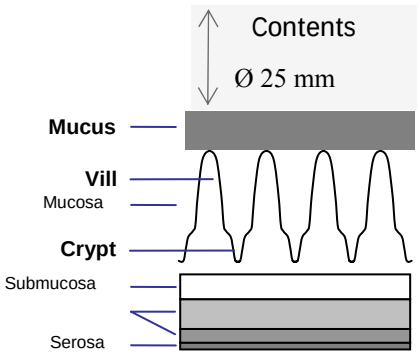

Figure 2. Schematic cross-section of the intestinal wall

A significant activity from the administered radiopharmaceutical may in some cases be excreted through the gastrointestinal tract. The absorbed dose to the intestinal wall and to the crypt cells might therefore be significant. Knowledge of the absorbed dose to the crypt cells is therefore important in the risk evaluation of a new therapeutic agent or in the optimization of a radiopharmaceutical used for diagnostic imaging. From a dosimetric point-of-view, it is important to determine the uptake of activity in the intestinal wall. Since it is virtually impossible to resolve the small intestinal wall from the intestinal contents in a nuclear medicine image, many dosimetrical models assume that the activity is only located in the contents (6, 7, 8, 10, 11). By experimental animal studies, the amount of activity in the intestinal wall and the contents can be measured through *in vitro* activity measurements of the excised organs (12).

The ICRP-model (6) and the MIRD-model (6) can be used to calculate the absorbed dose to the intestinal wall from the activity in the contents. Further development has been made by Stubbs *et al.* (10) and Poston *et al.* (11), who calculate the absorbed dose to different tissues in the intestinal wall.

Jönsson *et al.* (1) recently presented a new model to determine the absorbed dose to *villi* and crypt cells, when the activity is located in both the contents and in wall. The model also includes contribution from nearby intestinal loops. The electron and photon transport was simulated with EGS4.The small intestine was modeled as concentric cylinders, where the inner cylinder represents the small intestinal contents and the outer cylinder represents the intestinal wall. The small intestinal contents has a radius of 1.25 cm, whereas simulations were made with two wall thickness; 3 and 6 mm. Between the small intestinal contents and wall there is a thin layer of mucus. The thickness of this layer was difficult to obtain from the literature and therefore four values were used 5, 50, 100 and 200 μm. In order to calculate absorbed dose to the *villi* and crypt cells the outer cylinder was divided into three shells which represents the *villi* (500 μm), the crypt cells (150 μm) and the remainder of the intestinal wall. The activity was assumed to be homogenously distributed in the contents and also in the wall. All tissues in this model were treated as water equivalent, with a density of 1 g/cm^3.

Simulations to calculate the S values were performed for self and cross-dose from both wall and contents. The total S value was calculated as:

$$S_{total,wall} = S_{self,wall} + S_{cross,wall}$$
$$S_{total,contents} = S_{self,contents} + S_{cross,contents} \qquad \text{(Eqn. 7)}$$

The self-dose is the absorbed dose without contribution from nearby intestinal loops. This was simulated as an infinitive long cylinder, so the units were of the calculated S values were mGy MBq^{-1} cm^{-1} s^{-1}. To convert the S values to units of mGy MBq^{-1} s^{-1}, a length of the small intestine of 3 m was used. The geometry to simulate cross-dose from nearby loops is based on a simplified model of the complex geometry of the small intestine found in a patient. The model was defined as a hexagonal tube system consisting of 18 cylinders that enclose the target cylinder as shown in Fig. 3, since this is the most effective way to assemble cylinders. In the model, the tubes was set to 20 cm. However, simulations were performed for infinitive long cylinders (personal comment by Liu).

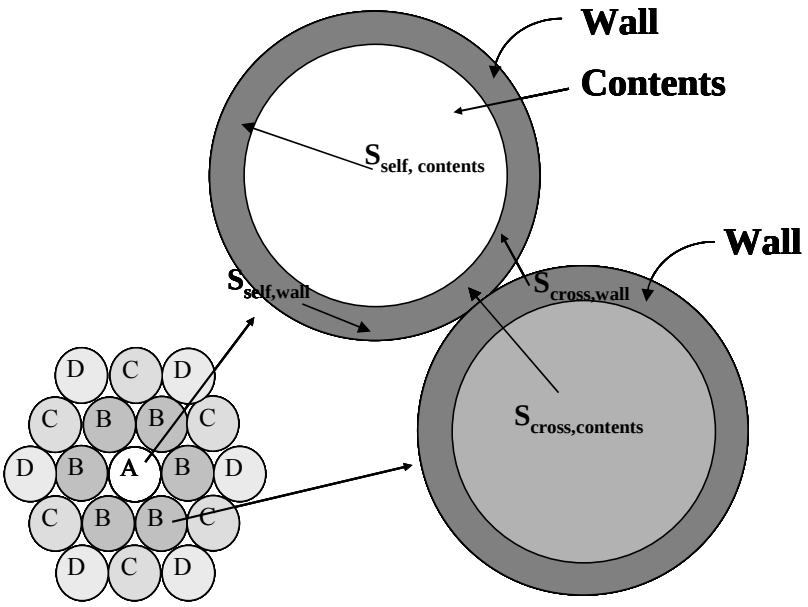

Figure 3. The model showing how self-doses and cross-doses from wall and contents are simulated. The self-dose is from activity in cylinder A only, with a infinitive cylinder length. Cross-dose simulations assume activity in all cylinders marked B, C and D with cylinder lengths 20 cm.

Simulations were made for monoenergetic electrons with energies of 0.2, 0.5, 0.8, 1, 2, 5, 8, 10 MeV, and for the radionuclides ^{99m}Tc, ^{111}In, ^{131}I, ^{67}Ga, ^{90}Y and ^{211}At. Since EGS4 only simulate photon and electron transport, the α-particle energy for ^{211}At was supposed to be locally deposited.

The investigation in this thesis is based on the model developed by Jönsson *et al.* (1) and previously described, but instead of the EGS4-code to simulate the particle transport the MCNP4c2 and MCNPX codes were used.

The Monte Carlo Technique

The Monte Carlo method is useful when analytic solutions to a problem are difficult or even impossible to derive. The method uses a random sampling generator to simulate transport of individual particles using their deterministic behavior. Photons and neutrons are ideal to simulate, whereas electrons that interacts with the long-range Coulomb force makes many small interactions are much harder to simulate.

The Monte Carlo-code used in this work for simulation of particle transport, including coupled neutron, photon and electron transport, is the general purpose MCNP (Monte Carlo N-Particle) code. An extended version also used in this thesis is the MCNPX code that also simulate proton and helium nuclei transport as well. The later can not be run under Windows environment which is the case for MCNP4c2.

MCNP physics

The detailed photon physics used in this work includes Compton (incoherent) scattering, coherent scattering, photoelectric effect and pair production. The Klein-Nishina formula is sampled exactly by Kahn's method below 1.5 MeV and by Koblinger's method above 1.5 MeV.

The electron transport in MCNP is mainly based on multiple-scattering theories describing angular deflections and energy-loss fluctuations. Since these theories rely on a variety of

approximations that restrict their applicability, they cannot solve the entire transport problem. In particular, it is assumed that the energy loss is small compared to the kinetic energy of the electron. The electron transport is arranged that the electron makes major energy steps where each energy step corresponds to a length of on the average 8.3% of its kinetic energy. However, to represent the electrons trajectory the energy steps must be divided into further substeps. Too few substeps in a material of interest could influence the electron transport and thereby the obtained result (13). The number of sub-steps can be changed with the parameter `[ESTEP]` and it is recommended that the number of sub steps in a geometric building-block, in MCNP referred to as a "cell", is at least 10 (13).

When the track of an electron crosses a surface, the transport is interrupted and the transport parameters are recalculated. The default procedure in MCNP works by way of assigning the transport parameters belonging to the previous energy step (MCNP-style energy indexing algorithm). This energy indexing algorithm introduces a systematic error (14, 15, 16). Another method for energy indexing, ITS-style is available in MCNP, which uses the transport parameters that belong to the energy step the nearest interruption. Comparisons with experimental data and other Monte Carlo codes show that simulations with the ITS-style energy indexing algorithm agrees better than if the MCNP-style was used.

Tallies

The desired information from a Monte Carlo simulation is obtained by a tally, *i.e.* predefined algorithms that score the contribution for each particle. MCNP tallies are normalized to be per starting particle and are printed in the output. MCNP4c2 and MCNPX have several different predefined tallies that the user can choose and modify. Examples of tallies can be deposited energy in a cell or a flux through a surface. The tallies `*F8` (MCNP4c2) and `+F6` (MCNPX) used in this work scores the deposited energy in a specified cell.

Uncertainties

The MCNP tallies are accompanied by a second number *R*, which is the estimated relative error defined to be one estimated standard deviation of the mean $S_{\bar{x}}$ divided by the estimated mean $\bar{x}$. In MCNP, the quantities required for this error will estimate the tally and its second moment, are computed after each complete Monte Carlo history, which accounts for the fact that the various contributions to a tally from the same history are correlated. For a well-behaved tally, *R* will be proportional to $1/\sqrt{N}$ where *N* is the number of histories. Thus, to halve *R*, we must increase the total number of histories fourfold. For a poorly behaved tally, *R* may increase as the number of histories increases.

Cell importance – Russian roulette

The geometry in MCNP usually consists of many cells. Cell importance, or Russian roulette, is a variance reduction method that can create several identical particles when a particle enters a cell. These are simulated as individual particles and the contribution to the tally is divided by the number of particles created + 1. For cells where few particles contribute to the tally, this can be a good method to keep the simulation times down.

Differences between MCNP4c2 and EGS4

The main advantage of MCNP4c2 over EGS4 is probably its advanced geometry coding tools (14). One drawback with MCNP compared to EGS4 is that the latter often runs a similar problem faster (15).
The differences between the two codes are mainly different cross sections and electron transport algorithms used. For MCNP the electron approximations are valid for an arbitrary angle while the algorithms used in EGS4 assumes the scattered angle to be small. For water

this tends to be no problem, but for high Z materials EGS4 underestimates the back scatter components (15). Many comparisons between the codes states that the results agree well when the ITS-style indexing algorithm is used for MCNP4 (15, 16).

For a more detailed review about MCNP see Appendix I.

Material and Methods

Intestinal Model

The model used in the present study is the novel model by Jönsson *et al.* (1) described briefly above. For simulation of the self-dose, a 300 cm cylinder represents the small intestine. Since no information regarding the surrounding material was found, a layer of 15 cm water surrounding the intestine (Fig. 4) was used. However, later it turned out that the simulations were performed using an approximately 7 cm water layer, why this surrounding also was used for the monoenergetic electrons and photons and radionuclides, but only for a wall thickness of 3 mm and mucus thickness of 5 μm.

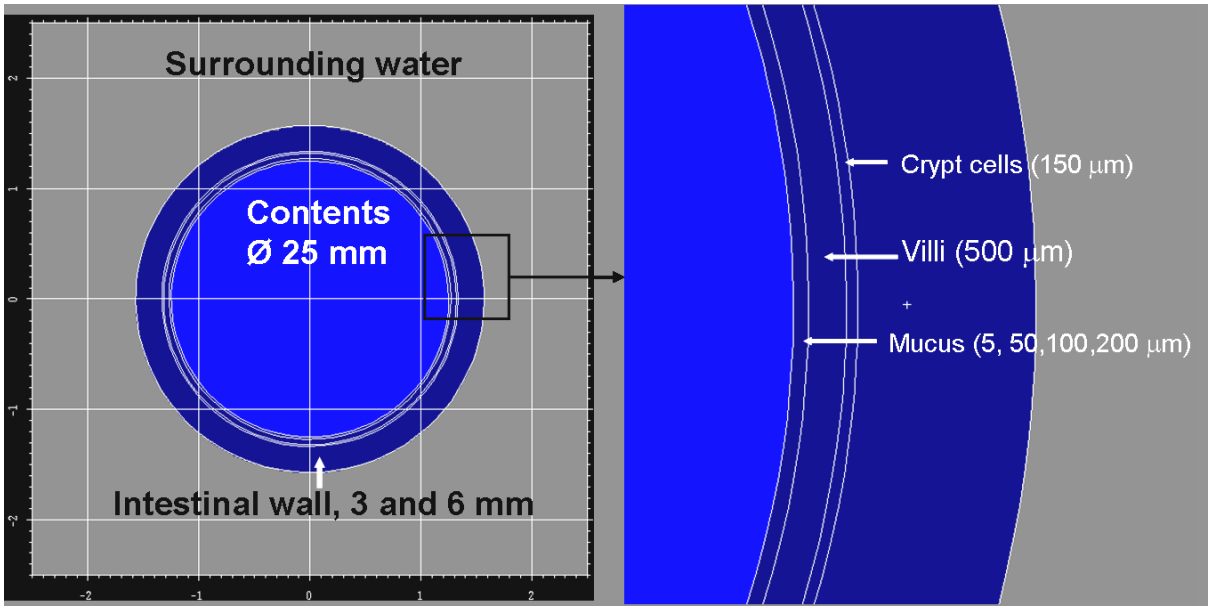

Figure 4. Screen-shot from the MCNP4c2 geometry plot describing the assigned geometry.

The model for cross-dose was represented by a hexagonal tube system with a length of each segment of 20 cm. This unit was centered in a 50 cm long elliptical cylinder (40x20) cm according to the description of the torso defined in MIRD pamphlet no 5 (17) illustrated in Fig. 5. Since the represented geometry for the simulations in (ref 1) consisted of infinitive long cylinders, to compare the simulations between the investigations, a geometry consisting of 100 m long cylinders (should be equal to infinitive) in 8 cm radius of water was also simulated using only a wall thickness of 3 mm and mucus thickness of 5 μm.

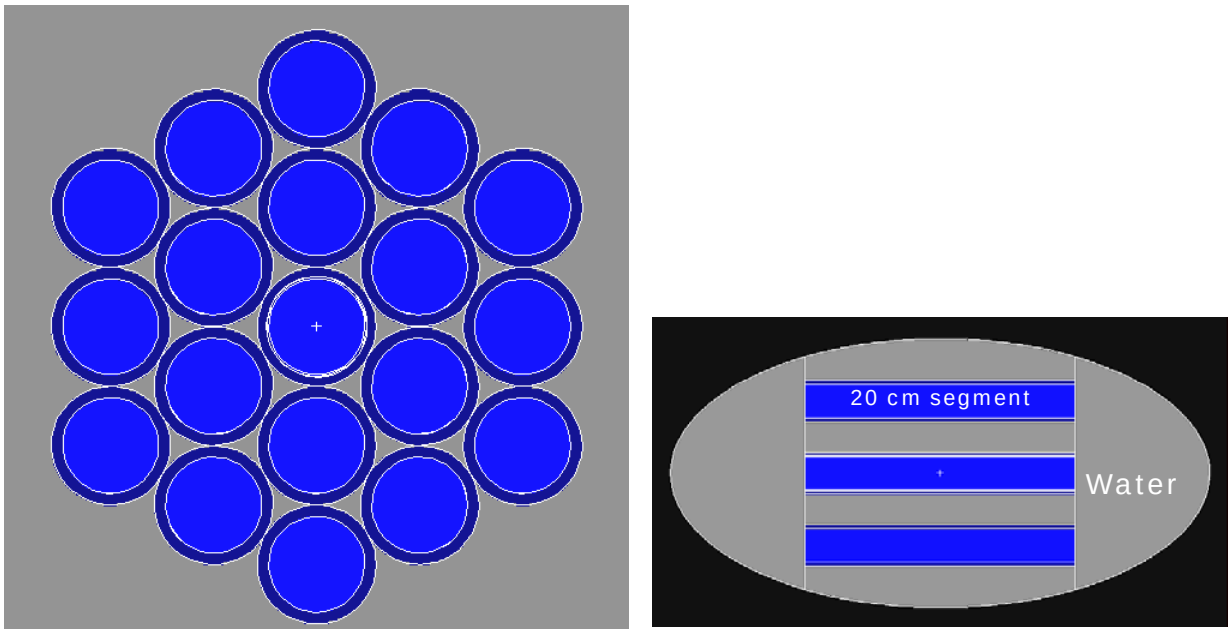

Figure 5. The geometry used in the simulation of the cross-dose. To the left a sagital cross-section and right a transversal cross section describing the placement of cylinders in the torso-shaped elliptical cylinder.

If the fraction of the cumulated activity in the whole small intestine that is located in the small intestine wall is defined as *f,* the absorbed dose to the crypt cell from the small intestine contents and wall can be described as:

$$D_{crypt \leftarrow wall} = \widetilde{A}_{wall} \cdot S_{crypt \leftarrow wall} = \widetilde{A}_{SI} \cdot f \cdot S_{crypt \leftarrow wall} \qquad \text{(Eqn. 8)}$$

$$D_{crypt \leftarrow contents} = \widetilde{A}_{contents} \cdot S_{crypt \leftarrow contents} = \widetilde{A}_{SI} \cdot (1-f) \cdot S_{crypt \leftarrow contents} \qquad \text{(Eqn. 9)}$$

The total absorbed dose from the small intestine (wall and contents) is the sum of Eqn. 8 and 9.

$$D^{total}_{crypt \leftarrow Small\ Intestine} = D_{crypt \leftarrow wall} + D_{crypt \leftarrow contents} = \qquad \text{(Eqn. 10)}$$
$$= \widetilde{A}_{Small\ Intestine} \cdot \left(f \cdot S_{crypt \leftarrow wall} + (1-f) \cdot S_{crypt \leftarrow contents} \right) =$$
$$= \widetilde{A}_{Small\ Intestine} \cdot S^{f}_{crypt \leftarrow Small\ Intestine}$$
$$, where\ S^{f}_{crypt \leftarrow Small\ Intestine} \equiv \left(f \cdot S_{crypt \leftarrow wall} + (1-f) \cdot S_{crypt \leftarrow contents} \right)$$

Simulations were made for monoenergetic electrons and photons, as well as for the radionuclides: ^{99m}Tc, ^{111}In, ^{131}I, ^{67}Ga, ^{90}Y and ^{211}At. The energies and yields were taken from MIRD (4), except for the ^{90}Y and ^{131}I beta spectrum, which was taken from Stabin *et al.* (5). The energy spectrum was tested versus unity density sphere phantoms described by Stabin *et al.* (5).

The self-dose from contents and wall were simulated for 0.05, 0.1, 0.2, 0.5, 0.8, 1, 2, 5, 8, 10-MeV electrons whereas the cross-dose from contents were simulated only for 1, 2, 5, 8 and 10-MeV, due to the short range of the electrons. The simulation time was defined to get an uncertainty of less than 2%, except for energies below 200 keV where the uncertainty was kept under 5 %. For photons, the self-dose from contents and wall and cross-dose from contents were simulated for 0.05, 0.1, 0.2, 0.5, 0.8, 1, 2, 5, 8 and 10-MeV photons. The simulation time was here also set to obtain an uncertainty of less than 2%.

The MCNP4c2 Monte Carlo code

All simulations were made with the MCNP4c2 Monte Carlo code, except for the α-particles where the MCNPX code was used. The electron transport was made with the ITS-style energy indexing algorithm instead of the default MCNP-style energy indexing algorithm by using the switch [DBCN 17J 1] in the input file.

For self-doses from the wall, and the simulations with photons, a conservative approach was used without any of the available variance reduction methods. For electrons that origins outside the wall, a conservative approach tends to be very time consuming, since only a few of the simulated electrons contribute to the tally. The variance reduction method of cell importance was used in the cells defining the mucus, *villi*, crypt cells and the remainder of the intestinal wall.

The tally used in the simulations for electrons and photons has been the `*F8:P` n or equally `*F8:E` n-tally. This tally record deposited energy in a cell, n, per event, E_{event}. The unit of the `*F8-` tally is MeV/event. Therefore the tally value must be converted to MeV/decay, which is done by multiplying the tally value with a probability for an arbitrary nuclear transition per decay, $p_{nuclear\ transition}$, divided by the probability of that bin, p_{bin}, found in the output-file. To calculate the self-dose S value, the deposited energy/decay is divided with the mass of the target, m_{target}, and is expressed in the units mGy MBq^{-1} s^{-1} as in (Eqn. 11).

$$\overline{S} = \frac{E_{event}(MeV)}{m_{target}(g)} \cdot \frac{p_{nuclear\,transition}}{p_{bin}} \cdot 0.1602 J \cdot g \cdot MeV^{-1} \cdot kg^{-1} \cdot MBq^{-1} \cdot s^{-1} =$$

$$= \frac{E_{decay}}{m_{target}} \cdot 0.1602\, mGy\, MBq^{-1}\, s^{-1} \qquad (eqn.\ 11)$$

Since the hexagonal tube model for cross-dose consisted of 19 segments of 20 cm each, the total length of the small intestine would be 3.80 m. For the model simulating self-dose the length of the cylinder was only 3m. The activity concentration ought to be equal in the two models calculating the S values so the cross-doses has to be corrected with a factor 380/300. Therefore the resulting equation for calculating cross-dose S values should be

$$\overline{S} = \frac{E_{decay}}{m_{target}} \frac{380}{300} \cdot 0.1602\, mGy\, MBq^{-1}\, s^{-1} \qquad (eqn.\ 12)$$

The simulation of the alpha particles from ^{211}At was made by the MCNPX-code, using the tally `+F6`. The unit of this tally is MeV/g/event, so the tally is already divided with the mass of the cell, which leads to Eqn. 13.

$$\overline{S} = E_{Event}(MeV) \cdot \frac{p_{nuclear\,transition}}{p_{bin}} \cdot 0.1602 J \cdot g \cdot MeV^{-1} \cdot kg^{-1} \cdot MBq^{-1} =$$
$$= E_{Event}(MeV) \cdot 0.1602\, mGy\, MBq^{-1}\, s^{-1} \qquad (eqn.13)$$

Since the range of the 5.867 MeV α-particles emitted from ^{211}At is less then 50 μm (19), no cross-doses have been simulated and the only mucus thickness simulated was 5 μm. MCNPX has an energy cut-off, the limit for simulation of alpha particles using cross-sections, as high as 4 MeV. For lower energies the continuously slowing-down approximation (CSDA) was used and no secondary electrons were simulated. The maximum energy for a secondary electron from a 5.867-MeV alpha particle, according to the physical rules of conservation of energy and momentum, is only about 0.8 keV since the difference between the masses of the electron and α-particle is about 10^4. This electron energy corresponds to a range in water less then 5 μm. Therefore these electrons do not contribute to either the cross-dose or self-dose from the contents.

Results & Discussion

Mono energetic electrons

Simulation of self-dose from monoenergetic electrons showed little importance of the radius of surrounding water. The, cross-dose using 100 m segments, agreed well with the data from Jönsson *et al.* (1) (from now on referred as (ref. 1)), except for 1 MeV electrons that were 10% less in this study. The difference might be due to different cross-section data between MCNP and EGS4 for the production of bremsstrahlung (19).

The result from the simulations of self-dose (15 cm surrounding tissue) and cross-dose (20 cm segments) to the crypt cells for monoenergetic electrons is shown in Fig. 6.

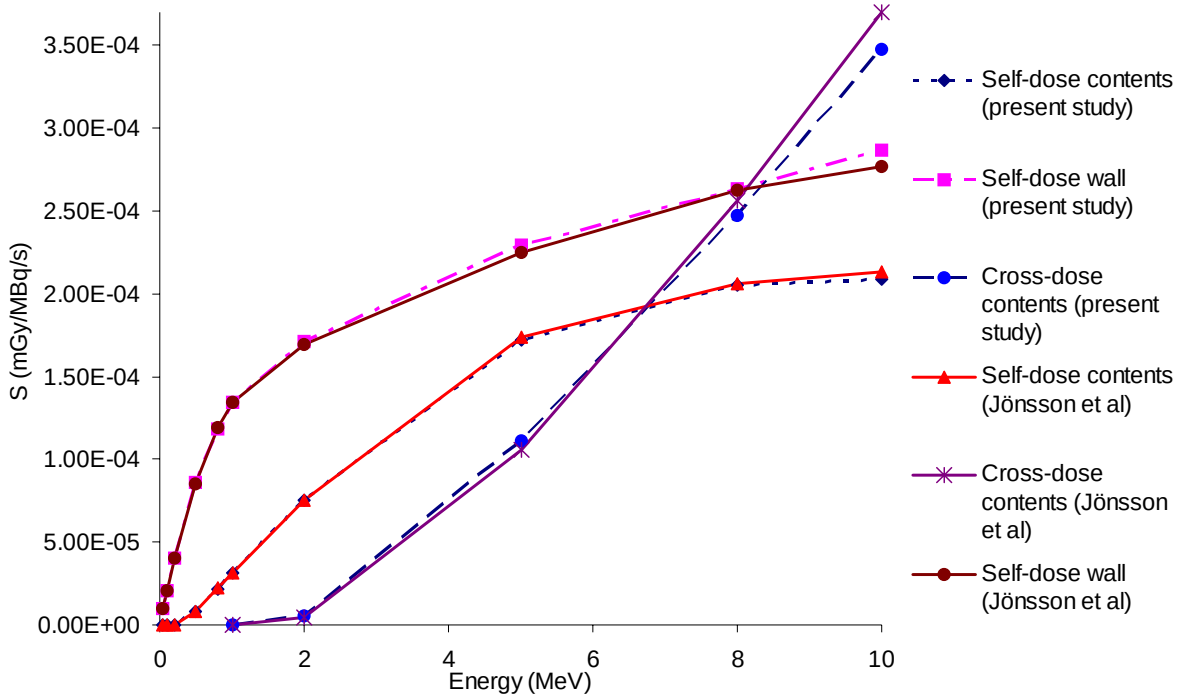

Figure 6. Self-dose (15 cm surrounding tissue) from wall and contents and cross-dose (20 cm segments) from contents from monoenergetic electrons to the crypt cells using a wall thickness of 3 mm and mucus thickness 5 μm.

For low energies below 0.5 MeV, the self-dose contribution from contents is negligible compared to contribution from the wall. For higher energies the contribution from contents becomes significant and for energies greater than 2 MeV the contribution is in the same order as from the intestinal wall with thickness 6 mm. The self-dose from wall with thickness 3 mm is higher than the one with 6 mm due to higher activity concentration. For low energies the difference is about a factor 2.2, but for higher energies and longer electron ranges the factor becomes about 1.3. These results show quite clearly that if only a few per cent of the cumulated activity from an electron emitter is located in the small intestine wall this could lead to a significant contribution to the absorbed dose. The contribution from cross-dose from contents to the total absorbed dose is not important for electrons under 2 MeV.

The difference in the self-dose from monoenergetic electrons in the intestinal wall, between the present study and (ref. 1) is within 2 %. The self-dose from contents is within a few of per

cent except for energies below 0.5 MeV. For these energies the short range electrons does not penetrate the *villi*. The absorbed fraction in the crypt cells is due to bremsstrahlung, and is a factor 1000 less than for 0.5 MeV, so the difference is small but the relative error for a 50 keV electron is as much as 300 %.

The results of the cross-dose simulations showed a good agreement with (ref. 1) for energies between 2 MeV and 5 MeV. For 1-MeV electrons the results from the present study are 25% lower, whereas 5 and 8 MeV electrons are 5% lower. The difference between the results depends mainly on the selection of the intestinal length, which was assumed to be infinite long cylinders in the study in (ref. 1). For 2 to 5 MeV electrons, this results in a small difference, due to the short range of the electrons. For 8 and 10 MeV electrons, the range of the electrons is so long that the geometry difference results in this significant difference. The CSDA-range of a 1-MeV electron is less than the needed 6 mm to penetrate two wall thicknesses. The contribution to the S value for 1 MeV is therefore due to bremsstrahlung or the small number of electrons that could penetrate to the crypt cells. However, since the S value for *villi* is the same as the S value for crypt cells, it is most probably due to the bremsstrahlung only. Since bremsstrahlung, is penetrating radiation, this imply that infinitive long cylinders results in higher values than the 20 cm long segments used in the present simulations.

Monoenergetic photons

Using 7 cm surrounding tissue (as in ref. 1) instead of 15 cm led to an average of 2-3% lower self-dose from both wall and contents, which is an effect of a lower back scatter contribution.

Using the cross-dose model with 100 m segments, led to values that were 17-34% higher (50 keV and 10 MeV respectively) than the data with 20 cm segments. The explanation for this is again the difference in the geometry setup. When considering a homogenous medium, the dose distribution should vary with ~1/r for an infinitive long cylinder (line source) in vacuum. For a cylinder with a length of 20 cm, this would act as an intermediate between a line source and a point source ($1/r^2$) leading to a higher result for the dose distribution around an infinitive long cylinder.

Photons are penetrating radiation and interact more sparsely than electrons leading a more uniform energy deposition around the source. Therefore, the thickness of the mucus is of less importance and simulations of S values with different mucus thicknesses could not be distinguished from each other.

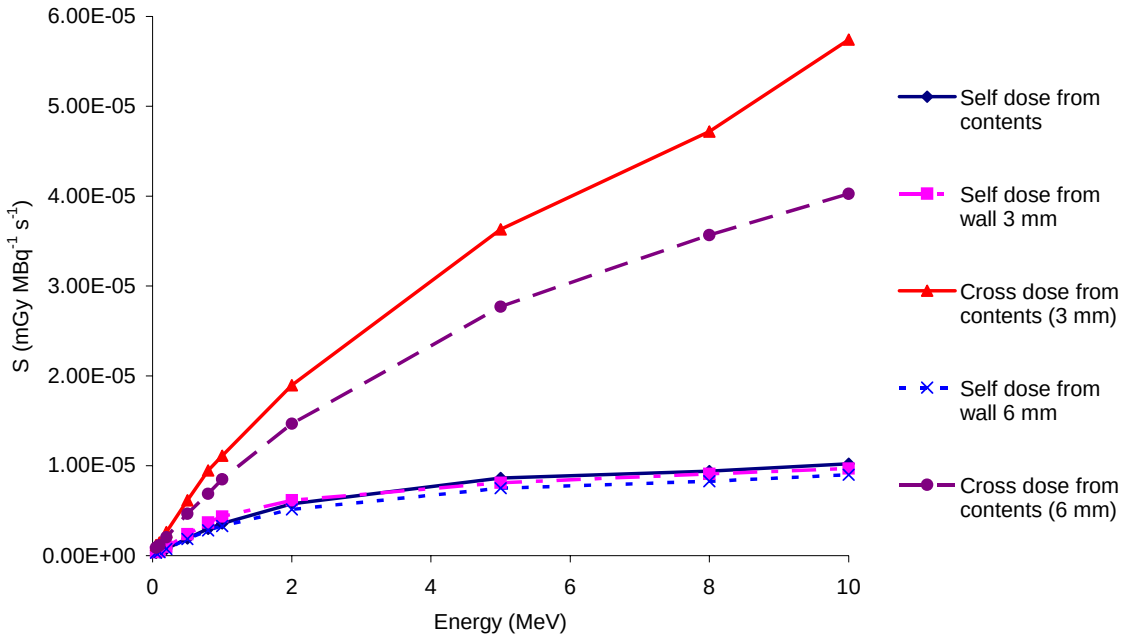

Figure 7. Self-dose and cross-dose from contents and self-dose from wall for monoenergetic photons using the more "realistic" geometries.

As can be seen in Fig. 7, the self-dose from the wall (15 cm surrounding water) for photon energies above 1 MeV is in the same magnitude as the self-dose from contents. For photons ranging from 50 keV to 1 MeV, the S values from wall with 3 mm thickness is about 20% higher than S values from the contents. This difference is only a few per cent if a wall thickness of 6 mm is used.

The cross-dose (20 cm segments) from contents (Fig. 7) is about a factor 3 higher than the self-dose for a 50-keV photon and a factor 6 for a 10-MeV photon. This is therefore the dominating contribution to the total S value. When the wall thickness is increased from 3 mm to 6 mm, the $S^{cross}_{contents}$ value is decreased by 20-30 %.

These results is in contradiction to the results obtained for the electrons with an energy less than 2 MeV, where it was found that there was a large difference (a factor 10^4 for energies below 200keV, and a factor 2.3 for 2 MeV) in the self-dose from wall S^{self}_{wall} and contents $S^{self}_{contents}$ and the cross-dose was negligible. For calculation of the absorbed dose for a radionuclide that emits both electrons and photons, it was found necessary to consider the uptake in the intestinal wall as well as the contribution from nearby loops of the small intestine. This clearly demonstrates the importance of the model developed by (ref. 1).

Radionuclides

As a step to check the agreement of the data with data from (ref. 1), the similar geometry was used. Except for ^{90}Y where the results agreed well, the difference in self-dose from contents ranged from being 6 to 12% higher in this study, this was a couple of percentage less than using a 15 cm radius. These results points towards that a even smaller radius was used in (ref. 1), and simulations showed that the studies agreed best if the radius was about 2.5 cm. Self-dose from wall was mainly due to electrons and was within 2% of (ref. 1), for simulations with and without x-rays. For 100 m cylinders, the difference in cross-doses from this study and Jönsson *et al.* (1) were in a span of 3 %.

A large activity uptake of the β-emitters ^{90}Y and ^{131}I in the intestinal wall tissue could lead to significant absorbed doses to the crypt cells (Fig. 8a). Due to the β-spectrum, the cross-dose from ^{90}Y will be smaller than expected when comparing to simulations with monoenergetic electrons. The large cross-dose contribution from the contents for ^{131}I is due to its photon emission component.

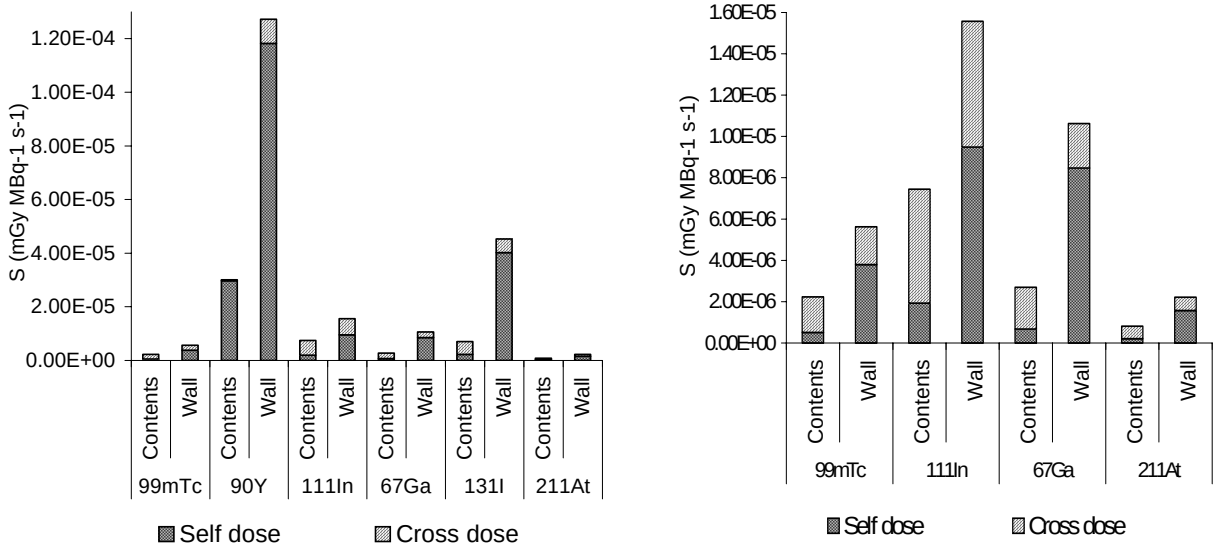

Figure 8. S values (mGy/MBq s) for crypt cells (wall thickness 3 mm, mucus 5 µm) using the geometries with 15 cm surrounding water and 20 cm segments.

a. All the studied radionuclides **b. Zoom of figure a without ^{90}Y and ^{131}I.**

*** Alpha particles in ^{211}At excluded**

Fig. 8b shows the importance of cross-dose for penetrating radiation and the fact that this dominates the contribution to absorbed dose from the contents for the radionuclide ^{99m}Tc, ^{111}In and ^{67}Ga. This can be predicted from the results of monoenergetic photons. The large difference (between 5 and 15.5 times (^{111}In and ^{67}Ga respectively)) in self-doses between the contents and the wall is explained by the additional contribution from conversion-electrons and Auger-electrons.

As seen in Fig. 9, when using the more realistic geometries than (ref. 1) there are some large differences in our results comparing to the data published by (ref 1). The results for self-dose from wall showed a good agreement (Fig. 9) and were within the uncertainties of 2%. The self-dose from contents were found to be 7-16% higher for all radionuclides except for ^{90}Y, where the results agreed well. The differences could partly be explained (about 2-3%) because of the different geometry setup as shown in the data from simulations with monoenergetic photons and discussed above.

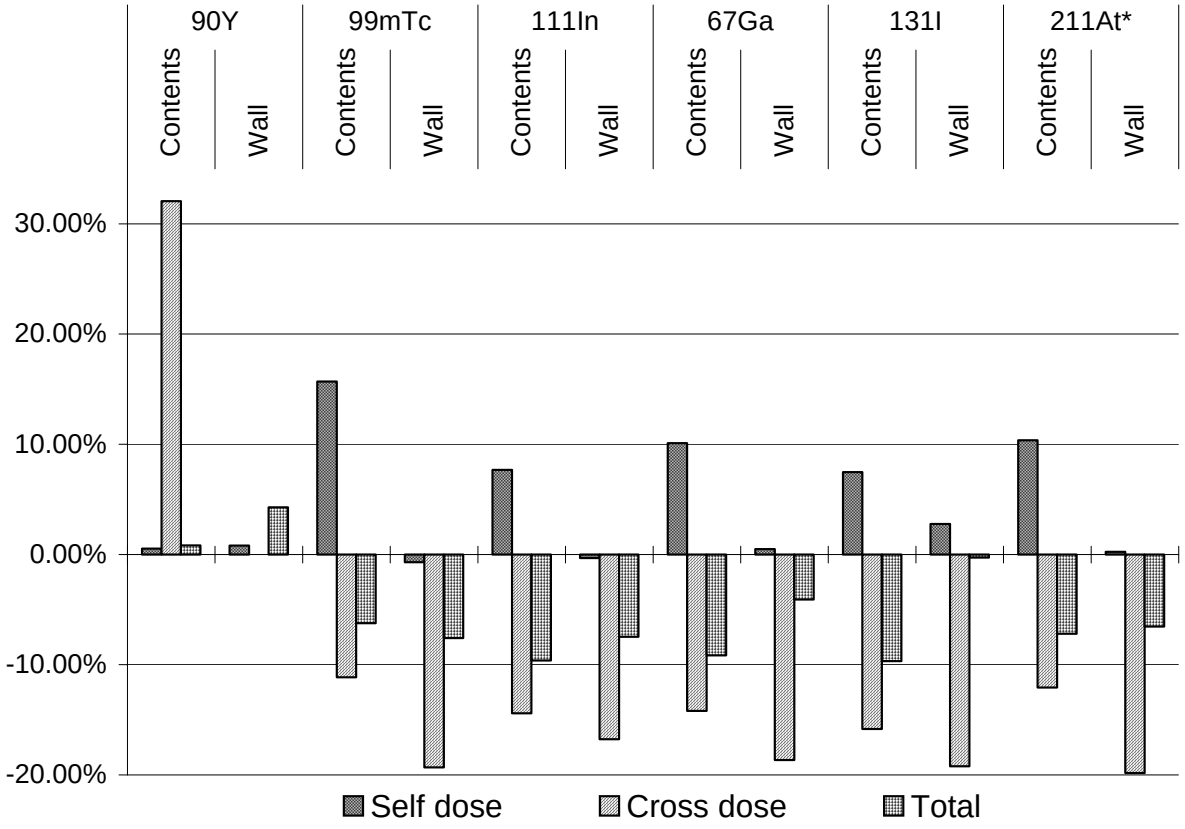

***No a-particles simulated for ^{211}At**

Figure 9. Comparison of data from simulations using MCNP4 (this study) and EGS4 (1).

The S values from cross-doses in the contents is in the range of 11-16 % lower compared to the values given in (ref. 1), and from the wall between 16-20% lower, except for ^{90}Y. For these radionuclides the electron range is less than the wall thickness so the cross-doses are mainly due to photons, so the differences is explained by the geometry difference and was predicted from the simulations with monoenergetic photons. The large difference in cross-dose from contents and ^{90}Y might depend on the differences in the shape of the tail of the β-spectra, since only electrons above 2 MeV contributes significantly to the S value. In the study of (ref. 1) no cross-dose from walls for ^{90}Y was simulated, which explains the difference between the columns corresponding to self-dose and total dose.

Fig. 10 shows a comparison of between results obtained from the present study and data from Jönsson *et al.* (1), ICRP (6), MIRD (7) and MIRDOSE 3 (8) respectively. For the present study and (ref. 1), the wall thickness was 3 mm and the mucus thickness was 200 μm. Our results and the data from (ref. 1) include contribution from the activity in the wall, resulting in a S values somewhere between the S values from wall and contents. The results for the present radionuclides show that the general models for the intestinal wall tend to overestimate the absorbed dose. The difference is even greater if the results from wall thickness of 6 mm are used instead of 3 mm.

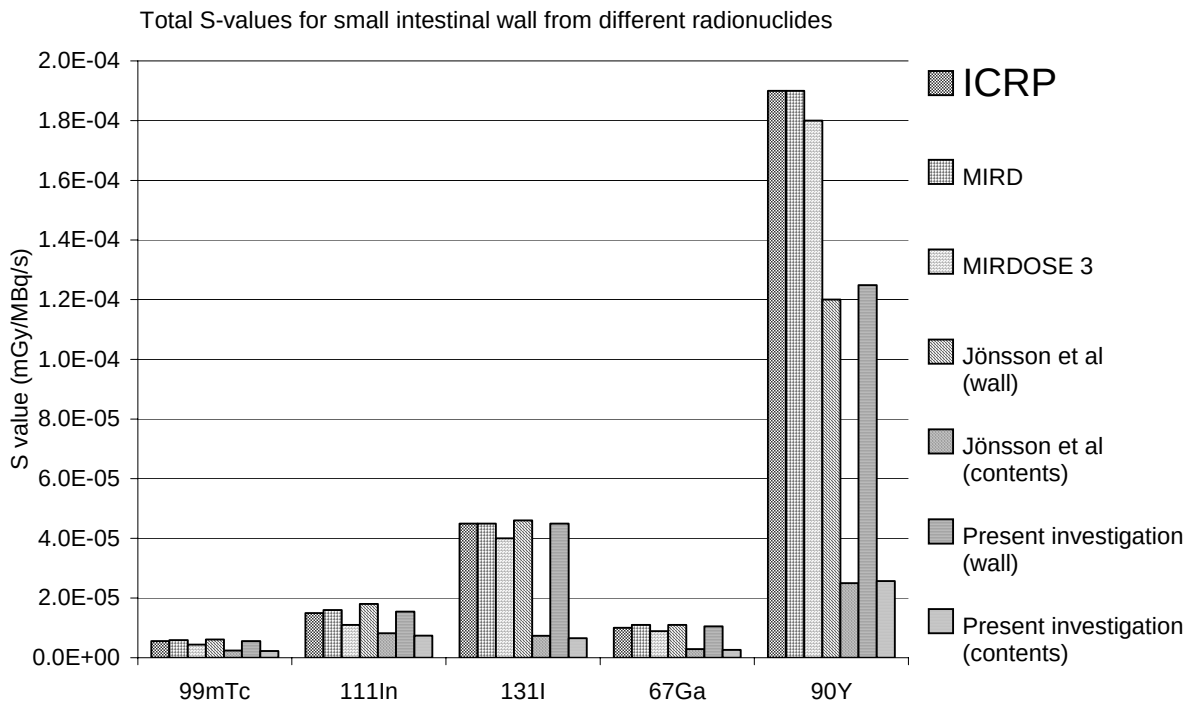

Figure 10. Total S value for the radionuclides studied, except for ^{211}At. For the models from ICRP (6), MIRD (7) and MIRDOSE3 (8) the S values are calculated for the intestinal wall, whereas for Jönsson *et al.* (1) and this investigation have S values are calculated for the crypt cells.

Alpha particles

The CSDA-range of a α-particle from ^{211}At is less than 50 μm. The mucus thicknesses used in this study were 5, 50, 100 and 200 μm. Thus, the only contribution to the absorbed dose in *villi* from alpha particles that origin from the contents is for 5 μm whereas the same contribution to the crypt cells always is zero. The result from the simulation is shown in table 1.

TABLE 1

S values for ^{211}At including alpha-particles

	$S_{e^-,\gamma}$ electrons and photons mGy MBq^{-1} s^{-1}			S_{α} α-particles mGy MBq^{-1} s^{-1}		
Target	Contents	wall (3 mm)	wall (6 mm)	Contents	wall (3 mm)	wall (6 mm)
*Villi**	$8.14\cdot10^{-7}$	$2.53\cdot10^{-6}$	$1.25\cdot10^{-6}$	$1.18\cdot10^{-6}$	$4.96\cdot10^{-4}$	$2.24\cdot10^{-4}$
Crypt cells*	$7.93\cdot10^{-7}$	$2.59\cdot10^{-6}$	$1.26\cdot10^{-6}$	0.00	$4.78\cdot10^{-4}$	$2.26\cdot10^{-4}$

* Mucus thickness 5 μm

The S value from contents to *villi* is not relevant since only the inner third of the *villi* will be irradiated by the α-particles. Thus, the absorbed dose will be very inhomogeneous and the magnitude very much dependent on the variation of the mucus- and *villi* thicknesses.

The most interesting result was found in the large difference in S value when the activity was located in the wall or in the contents. For example, when the wall thickness was 3 mm, we found a difference of a factor of 200 between S values from activity in wall compared to when the activity is in the contents. As for the electrons, the α-particle self-dose from wall is about 50% lower for a 6 mm wall compared with a 3 mm wall.

It requires only a few, 1-4 α-particles that traverse through a mammalian cell nucleus to sterilize a cell (20). Therefore, the absorbed dose quantity from α-particles may not be a satisfied quantity for risk estimation due to its stochastic behavior. However, the S values shown in Table 3.1 indicate that knowledge of the mucus thickness and especially the absorption in the wall is of greatest importance in the determination of the radiation risks with α-particle therapy based on radionuclides that excreted through the GI-tract.

In the investigation by Jönsson *et al.* (1), the energy of the α-particles is considered to be locally absorbed. Assuming this yields an S value from α-particles of $4.95\cdot10^{-4}$ mGy MBq^{-1} s^{-1} for a 3 mm wall. This is in a good agreement with the S value for *villi* in this study. The S value for crypt cell in this study shows to be about 4 % lower than from the data of Jönsson *et al.*

Conclusion

The aim of this work has been to implement and evaluate the MCNP4c2-code in the field of small-scale dosimetry. The comparison of our results with the study published by Jönsson *et al.* showed differences that mainly can be explained by the difference in the geometry setup, except self dose from contents. Therefore, the aim of this study has been fulfilled and the

results shows that this code in combination with its possibility to define complex geometries can be a useful tool in future research of small scale dosimetry models.

The dimension of cells should not be smaller than the length of an energy step, since this could lead to a larger energy deposition. This could be a problem for ^{90}Y, which first energy step will be about 0.9 mm. By combining the cell that define the crypt cells with the cell that defines *villi*, the energy deposition in this cell was the same as for the sum of the two separate cells.

The results for the monoenergetic electrons and photons indicate the important factors in this model. For penetrating radiation, the activity uptake in the wall lead to S values in the same magnitude as radiation coming from the contents. On the other hand, for electron with energies below 5 MeV this uptake in the wall is of great importance.

For photons, the dominating contribution to the total absorbed dose from the small intestine is the cross-dose. This effect is, on the other hand, is negligible for electrons under 1 MeV and low under 2 MeV.

An assumption in this model has been that the activity is regarded as uniformly distributed in both the wall and the contents. Any heterogenic activity distribution in the wall could lead to significant changes in the absorbed dose to the crypt cells both on a tissue and cellular level as explained in the next chapter.

Limitations with the MIRD scheme

As has been mentioned previously, the mean absorbed dose in an organ is not directly correlated to a biological effect of the radiation. The absorbed dose can vary greatly within an organ due to heterogenic distribution of the radiopharmaceutical in either the source or the target regions. This then alter the cross-dose - a contribution that is largest closest to the source organ. To avoid this problem, 3-D absorbed dose distribution must be calculated for example by using a 3-D activity quantification table together with CT-slices to create a voxel based geometry input for a Monte Carlo code. The main drawback of this method could be the long calculation time, but there is about a week of simulation time during the activity quantification is performed and with the faster going computer technology and possibilities to connect computers into a cluster, this problem could be solved. With the scintillation cameras used today the resolution of the quantified activity could be measured with a resolution of about 1 cm, and the activity is an average over this voxel. For an organ with known 3-D dose distribution the DVH (dose volume histogram) could be an important factor to quantify the effect of the tissue.

Even though the 3-D dose distribution is known, it's still an average absorbed dose with a resolution about 1 cm, or approximately 1000 cell radius, due to the spatial resolution of the gamma camera. To correlate the absorbed dose with an effect, the distribution of the radiopharmaceutical on a cellular level has to be studied. For example if a radiopharmaceutical, marked with a low-range Auger electron emitters, is present only in a certain type of cells within an organ the effect on these cells could be great while the mean absorbed dose over the tissue still could be low.

It's also important to consider the intracellular activity distribution to determine the radio-toxicity of the radiopharmaceutical. For example, the radionuclide ^{125}I emits 25-30 Auger electrons per decay that have very low energies and subsequently high stopping-power. These electrons contributes little to the mean absorbed dose, and if the radiopharmaceutical is present outside the cell nucleus the short range of these Auger electrons results in a limited effect on the cells. On the other hand, if the radiopharmaceutical is incorporated in the DNA-helix then the Auger electrons could contribute to a significant effect (21).

If the dose rate is low, cells have greater possibility to repair possibly lethal damages (PLD), while with higher dose rate the repair mechanism is less effective and the radiation effect increases with dose rate. The MIRD-formalism does not take this dose rate effect in consideration, which is a very important parameter for early radiation effect. This is because the formalism was developed mainly to estimate the absorbed dose for diagnostic imaging, where the administrated activity is low and the effect of importance is late responding. However, for higher activity used in radionuclide therapy, the biological effect versus the dose rate will be significant.

Future work

An interesting future research field is the application of the Monte Carlo technique for small scale dosimetry based on images obtained by autoradiography on heterogeneous dose distributions in, for examples, the spleen and testis (12). This may be possible to do if one creates either a voxel-based geometry built on images from autoradiography or adaptation of Boolean algebra to represent a model based from the same images. If this could be achieved using the MCNP code is a task that depend on many factors. The first problem is that MCNP only can simulate photons as well as electrons above 1 keV. Below this threshold, the particle is assumed to be absorbed. Another problem can be that many cell boundaries affect the electron transport. To overcome this, one could treat the volume as water-equivalent material and avoid dividing the volume into small cells. Instead of the *F8-tally that requires the cell boundary definition, one could use the F4-tally to determine electron fluence. This tally allows a cell to be subdivided into up to 1000 segments. The tally can then be converted to deposited energy by multiplying with the stopping power as has previously been described by Schaart *et al.* (18). The problem that arises then is how to specify the source.

References

1. Jönsson L, Liu X, Jönsson BA, Ljungberg M, Strand SE. *A Dosimetry Model for the Small Intestine Incorporating Intestinal Wall Activity and Cross-Doses.* J. Nucl. Med. 43 **(2002)** 1657–1664.
2. International Commission on Radiation Units and Measurements. *Absorbed-Dose Specification in Nuclear Medicine.* ICRU Report 67. Journal of the ICRU Volume 2, No 1, 2002; Washington, D.C., **2002**.
3. Loevinger R, Budinger T F, Watson E E. *MIRD Primer for Absorbed Dose Calculations*; The Society of Nuclear Medcine Inc.: New York, **1988**.
4. Weber DA, Eckerman KF, Dillman LT, Ryman JF. *MIRD: Radionuclides Data and Decay Schemes*; The Society of Nuclear Medicine: New York, **1989**.
5. STABIN MG. *www.doseinfo-radar.com*
6. International Commission on Radiological Protection. *Limits for Intakes of Radionuclides by Workers.* ICRP Publication 30: Part 1. New York, NY: Pergamon Press; **1979**.
7. Snyder WS, Ford MR, Warner GG, Watson SB. *"S," Absorbed Dose per Unit Cumulated Activity for Selected Radionuclides and Organs*. MIRD Pamphlet No. 11. New York, NY: Society of Nuclear Medicine; **1975**.
8. Stabin M. *MIRDOSE: personal computer software for internal assessment in nuclear medicine*. J. Nucl. Med. 37 **(1996)** 538–546.

9. Potten CS. *Radiation, the Ideal Cytotoxic Agent for Stydying the Cell Biology of Tissues such as the Small Intestine.* Radiat. Res. 161 **(2004)** 123-136.

10. Stubbs JB, Evans JF, Stabin MG. *Radiation absorbed doses to the walls of hollow organs.* J. Nucl. Med. 39 **(1998)** 1989-1995.

11. Poston JW Jr, Kodimer KA, Bolch WE, Poston JW Sr. *A revised model for the calculation of absorbed energy in the gastrointestinal tract.* Health Phys. 71 **(1996)** 307-314.

12. Jönsson BA, Strand SE, Larsson BS*A. Quantitative Autoradiographic Study of the Heterogeneous Activity Distribution of Different Indium-111-Labeled Radiopharmaceuticals in Rat Tissues.* J. Nucl. Med. 33 **(1992)** 1825-1833.

13. Briesmeister JF, Ed., *"MCNP - A General Monte Carlo N-Particle Transport Code, Version 4C,"* LA-13709-M (April **2000**)

14. Chibani O and Li XA "*Monte Carlo dose calculations in homogeneous media and at interfaces: A comparison between GEPTS, EGSnrc, MCNP, and measurements"* Med. Phys. 19 (5) **(2002)** 835-847

15. Jeraj R, Keall PJ, Ostwald PM. *Comparisons between MCNP, EGS4 and experiment for clinical beams.* Phys. Med. Biol. 44 **(1999)** 705-717.

16. Schaart DR, Jansen JTM, Zoetelief J, de Leege PFA. *A comparison of MCNP4C electron transport with ITS 3.0 and experiment at incident energies between 100 keV and 20 MeV: influence of voxel size, substeps and energy indexing algorithm.* Phys. Med. Biol. 47 **(2002)** 1459-1484.

17. Snyder WS, Ford MR, Warner GG. *Estimates of specific fractions for photon sources uniformly distributed in various organs of a heterogeneous phantom.* MIRD Phamphlet No. 5 (revised). New York, NY: Society of Neclear Medicine; **1978**.

18. The International Commission on Radiological Protection *ICRU Report 49 Stopping Powers and Ranges for Protons and Alpha Particles*; **(1993)**.

19. Siebers JV, Keall PJ, Libby B, Mohan R. Comparison of EGS4 and MCNP4b Monte Carlo codes for generation of photon phase space distribution for a Varian 2100C. Phys. Med. Biol. 44 **(1999)** 3009-3026.

20. Charlton DE, Kassis AI, Adelstein SJ. *A comparison of experimental and calculated survival curves for V79 cells grown as monolayers or in suspension exposed to alpha irradiation from ^{212}Bi distributed in the growth medium.* Radiat. Prot. Dosim. 52 **(1999)** 311-15.

21. Kassis AI, Sastry KSR, Adelstein SJ. *Kinetics of uptake, retention, and radiotoxicity of ^{125}IUdR in mammalian cells: implications of localized energy deposition by Auger processes.* Radiat. Res. 109 **(1987)** 78-89

Appendix

MCNP

A brief survey of the MNCP code is given below. For details see (14).

Photon physics

For all elements from Z = 1 through Z = 94 the photon interaction tables are based on evaluated data from ENDF from 1 keV to 100 MeV. Fluorescence data are taken from work by Everett and Cashwell. The Klein-Nishina formula is sampled exactly by Kahn's method below 1.5 MeV and by Koblinger's method above 1.5 MeV.

The generation of electrons is handled in three ways.

- Mode P E - All interaction except coherent scatter can result in an electron. This is stored for later transport.
- Mode P - The electron transport is turned off. Any possible electron assumes to travel in the same direction as the incident photon and is immediately absorbed. A thick target bremsstrahlung model (TTB) is used. Any photons produced by the electron are stored for later transport.
- IDES = 1 - All electron production is turned off and no bremsstrahlung is created either, and all electron energy is assumed to be locally deposited.

There are two different modes (simple and detailed) that can be chosen and they treat the photon physics a little bit different:

- Simple – ignores coherent scatter and fluorescent photons from photoelectric absorption
- Detailed – includes incoherent (Compton) scattering, coherent scattering (no energy loss), photoelectric effect and pair production. This is the default method used in MCNP.

Electron Physics

When a photon with energy of 0.5 MeV is followed down to about 60 keV in aluminum, it undergoes fewer than 10 interactions. An electron interacts with the long range Coulomb force, so it undergoes many interactions with small energy loss per interaction. For the same example but for an electron the number of interaction would be around 10^5 individual interactions. The many number of interactions would make the simulations very complicated resulting in long simulation times. Therefore many analytic and semi analytic methods have been developed for multiple-scattering theories.

The electron transport in MCNP is based mainly on Goudsmit-Saunderson theory for angular deflections, the Landau theory of energy-loss fluctuations, and the Blunck-Leisegang enhancements of the Landau theory. These theories rely on a variety of approximations that restrict their applicability, so that they cannot solve the entire transport problem. In particular, it is assumed that the energy loss is small compared to the kinetic energy of the electron. The

electrons energy loss and angular deflection during each energy step are sampled from probability distributions based on the appropriate multi-scattering theories. This accumulation of many individual collisions into single steps constitutes the "condensed history" Monte Carlo method. The electron physics is essentially that of the Integrated TIGER series (ITS).

On the average the energy and path length are related by

$$E_{n-1} - E_n = -\int_{s_{n-1}}^{s_n} \frac{dE}{ds} ds$$

where $-dE/ds$ is the total stopping power in energy per unit length and depends on the energy and the material in where the electron is moving.

The transport of electrons in MCNP is structured so that the electrons make major steps with predetermined path lengths s_n such that on the average

$$\frac{E_n}{E_{n-1}} = k$$

, where n is the electron energy at the end of the nth major step and k equals $2^{-1/8}$. This leads to an average energy loss of 8.3% per major energy step as seen in Fig. 1.

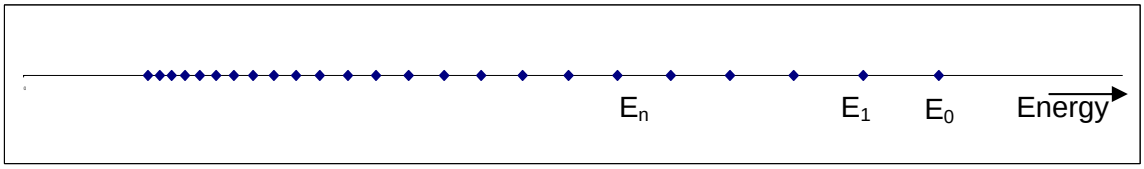

Figure 1. Major energy steps.

When an electron crosses a cell boundary the major energy step is interrupted and a new energy step starts. MCNP can handle this in two ways; MCNP- or ITS-style energy indexing algorithm.

-MCNP-style energy indexing algorithm. Assigns the transport parameters from the energy group for which the electron energy lies in between the group boundaries.

-ITS-style energy indexing algorithm. Assigns the transport parameters from the energy group whose upper boundary is closest to the electron energy.

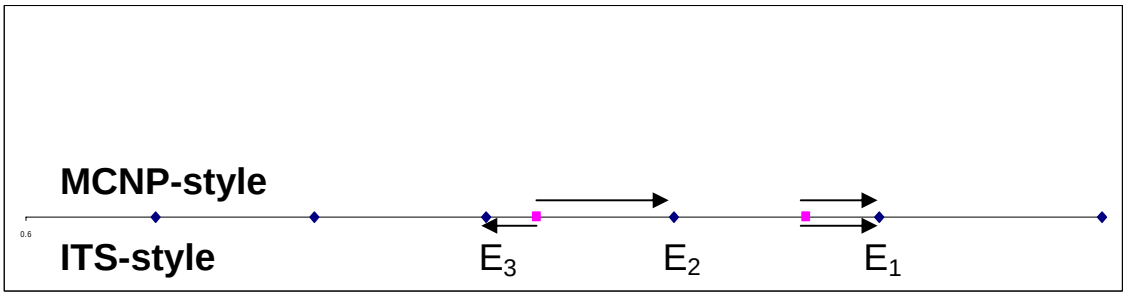

Figure 2. Shows the difference between how the MCNP- and ITS-style energy indexing algorithm treat a major energy step interrupted by a cell boundary.

The Fig. 2 shows the difference between the ITS- and the MCNP-style indexing algorithm, when a major energy step is interrupted by a cell boundary. The MCNP-style therefore introduces a systematic error. In order to represent the electrons trajectory more accurately,

the energy steps must be divided into further substeps with length of $\frac{s_n}{m}$. The default value for water is 3. In some circumstances it is desirable to increase the value of m for a given material. Especially very small regions may not accommodate enough number of substeps to represent the electrons trajectory. A reasonable rule of thumb is that an electron should make at least 10 substeps in any material of importance to the transport problem.

Alpha particle physics

The energy cutoff for alpha particles in MCNP is 4 MeV, and then the CSDA is used. No bremsstrahlung photons or knock-on electrons are therefore simulated. The amount of produced bremsstrahlung photons below 4 MeV is negligible and any produced knock-on electron would travel less then 5 μm in water.

Geometry setup

The geometry specification is important for setting up a proper model describing the problem. The methods in MCNP allow the user to define cells that together create the model. The cells are defined by complements and subsets of one or many surfaces. The surfaces are described by Boolean geometry of the 4th grade and could be planes in space, spheres, ellipsoids, cylinders, thyroids etc.

Each cell is described by a cell card defining the geometry. This cell card also contains information of the density of the cell and a link to a material card that specifies the atomic composition.

Source specifications

To specify the source the geometry, the type of particle (only one at the time), energy or energies with corresponding probabilities or energy distributions must be specified.

Tallies

In this work the F8-tally has been used. With an asterisk in front of this tally (*F8) the tally has been converted from register deposition of pulses to deposition of energy (MeV) in a cell.

For MCNPX the corresponding tally is the F6-tally. With a + sign in front of the tally (+F6) the tally register totally deposited energy from all types of particles in a cell divided with the cell mass and is displayed in the units MeV/g.

Variance reduction

For a simulation where there is a low probability for a particle to contribute to the tally, the low efficiency could lead to long simulation times. For these reasons one can speed up the efficiency by using different kind of variance reduction. The only one used in this work is based on cell importance and is therefore explained in more detail.

- Cell importance – When a particle from a cell with cell importance 1 enters a cell with cell importance (weight) 10, this one particle becomes ten identical particles. If the

particle contributes to the tally the contribution is divided with the particle weight. When a particle leaves the cell to a cell with cell importance of, for example two, Russian roulette is performed and the particle has a chance of 1/5 to survive.

Example of input file

Input file for simulation of self-dose from wall for ^{99m}Tc photons for a wall thickness of 6 mm and mucus thickness 200 μm.

```
1.  MESSAGE: IXR outp=r\wpho1 r=r\wph1

2.  Photons 99-Tc-m S(self,wall) 6 mm
3.  C CELL CARDS
4.  1   3  -1 2 -1 -3        imp:p=1   imp:e=1 $ Small intestine contents 3 m
5.  2   1  -1 2 1 -4 -3      imp:p=1   imp:e=1 $ Mucus 200 µm
6.  3   1  -1 2 4 -5 -3      imp:p=1   imp:e=1 $ Villi 0.5 mm
7.  4   1  -1 2 5 -6 -3      imp:p=1   imp:e=1 $ Crypt cells 0.15 mm
8.  5   1  -1 2 6 -7 -3      imp:p=1   imp:e=1 $ Remainder of intestinal wall 5.35 mm
9.  6   2  -1 2 7 -8 -3      imp:p=1   imp:e=1 $ Extra layer 2 cm to simulate electron transport
10. 7   2  -1 10 -2 -8       imp:p=1   imp:e=1 $ 5 cm water at the end
11. 8   2  -1 -11 3 -8       imp:p=1   imp:e=1 $ 5 cm water at the other end
12. 9    2  -1 10 8 -9 -11  imp:p=1   imp:e=0 $ Surrounding water e-transport försummas
13. 10   0   -10:9:11        imp:p=0  imp:e=0  $ Zero-importance outside world

14. C SURFACE CARDS
15. 1   CX  1.25
16. 2   PX  -150
17. 3   PX  150
18. 4   CX 1.27
19. 5   CX 1.32
20. 6   CX 1.335
21. 7   CX 1.87
22. 8   CX 3.87
23. 9   CX 15
24. 10  PX -155
25. 11  PX 155

26. C    D A T A - cards
27. C    ============================
28. C MATERIALS:
29. C  Water
30. M1  1001.02P 2 8016.02P 1 $Material card, 2 parts H and 1 part O makes H2O
31. M2  1001.02P 2 8016.02P 1 $ estep=n Number of sub-steps
32. M3  1001.02P 2 8016.02P 1
```

```
33.     C
34.     C SOURCE:
35.     SDEF ERG=D1 PAR=2 AXS=1 0 0 EXT=D2 RAD=D3
36.     SI1 L 0.140500     $ Photon energies 99-Tc-m
37.           0.018370
38.           0.018250
39.           0.020600
40.     SP1   0.891000     $ Corresponding probabilities
41.           0.040100
42.           0.021100
43.           0.012300
44.     SI2 -150 150       $ Extension of cylinder source along x-axis (cm)
45.     SP2 0 1            $ Uniform distribution along the extension
46.     SI3 1.27 1.57      $ Source in the wall (cm)
47.     C
48.     C GENERAL:
49.     MODE P E           $ Simulates both photon and electron transport.
50.     DBCN 17J 1         $ ITS-style energy indexing algorithm
51.     C
52.     C TALLIES:
53.     FC8 Dep energy (MeV) $Tally comment card, inserted in output-file
54.     *F8:P 3 4          $Deposited energy (MeV) in cell 3 and 4
55.     C
56.     C Run limits:
57.     NPS 3000000        $Number of particles simulated
58.     C CTME 30          $End simulation after 30 min of computer time (comment)
```

Short explanation of the input file

The numbers 1-58 are added to simplify this explanation and should not be a part of the input-file. The first line is optional, but it tells us that we want to check the code for errors, load cross-sections and run the problem. The output files are created in a subfolder called R, since many simulations creates many output files. Line two is optional and is only a message line. A line starting with C means it is a comment and is ignored by the program. When a $-sign appears the program ignores the rest of the line so it could be useful for making comments.

Line 4 – 13 defines the cells. The first entry names the cell and the second entry calls the material card on line 30 – 32. A zero means vacuum and no density should be entered. The third entry defines the density of the cell (-1 = 1 g/cm^3). The next entries define how and what surfaces that builds up the geometry of the cell. A positive sign means either outside a sphere, cylinder etc or for planes on the positive side of the plane and a minus sign means the opposite. The imp:p=1 imp:e=1 means that the importance (weight) is 1 for both electrons and photons, meaning for every particle that enters the cell one particle should be continued simulated. In cell 9 the imp:e=0 indicate the desire to not want to follow that electron anymore and cell 10, defining the outside world, has particle weight zero for both electrons and photons.

Line 14 - 25 is the surfaces used to create the whole geometry. The first entry is the name of the surface and the second defines what type it is. CX is a cylinder along the x-axis and PX is a plane orthogonal to the x-axis. For CX the next entry defines the radius of the cylinder whereas for PX it defines the x-coordinate.

Example: Cell 1 is made of material 3 with density 1 g/cm3 and is inside surface 1, on the positive side of surface 2 and on the negative sign of surface 3. The cell therefore defines a cylinder with radius 1.25 and extension from -150 to 150 along the x-axis. This cell therefore defines the intestinal contents.

Line 30 – 32 defines the material and is explained on line 30. The entry estep=n defines the number of sub-steps used in the material (default for water = 3).

On line 35 starts the definition of the source. ERG is the energy and D1 is a link to SI1 (source information) and SP1 (source probabilities). PAR = 2 means that we want to simulate photons (PAR = 3 creates electrons). Only one particle type can be generated in the source. AXS = 1 0 0 means that the source is extended along the x-axis, and EXT defines the length of extension. RAD is the radii between which the source is generated.

Mode P E and DBCN 17J 1 describes that both electron and photon-transport should be simulated using the ITS-style energy indexing algorithm.

The lines 53 and 54 defines the tally to register deposited energy in cell 3 (*villi*) and 4 (crypt cells). The last two lines sets the number of histories to be run or if the simulation should end after a certain computer time.